Preparation of a supplementary cementitious material through synergy CO_2 mineralization of fly ash and carbide slag

Zhang, Hongzhi; Shao, Yingxuan; Ma, Chuanyi; Meng, Xianglong; Jiang, Nengdong; Ge, Zhi; Liang, Meijun; Chang, Honglei; Šavija, Branko

DOI
10.1080/21650373.2024.2441463

Publication date
2024

Document Version
Final published version

Published in
Journal of Sustainable Cement-Based Materials

Citation (APA)
Zhang, H., Shao, Y., Ma, C., Meng, X., Jiang, N., Ge, Z., Liang, M., Chang, H., & Šavija, B. (2024). Preparation of a supplementary cementitious material through synergy CO_2 mineralization of fly ash and carbide slag. *Journal of Sustainable Cement-Based Materials*, *14*(6), 1073-1088. https://doi.org/10.1080/21650373.2024.2441463

Journal of Sustainable Cement-Based Materials

ISSN: (Print) (Online) Journal homepage: www.tandfonline.com/journals/tscm20

Preparation of a supplementary cementitious material through synergy CO_2 mineralization of fly ash and carbide slag

Hongzhi Zhang, Yingxuan Shao, Chuanyi Ma, Xianglong Meng, Nengdong Jiang, Zhi Ge, Meijun Liang, Honglei Chang & Branko Šavija

To cite this article: Hongzhi Zhang, Yingxuan Shao, Chuanyi Ma, Xianglong Meng, Nengdong Jiang, Zhi Ge, Meijun Liang, Honglei Chang & Branko Šavija (17 Dec 2024): Preparation of a supplementary cementitious material through synergy CO_2 mineralization of fly ash and carbide slag, Journal of Sustainable Cement-Based Materials, DOI: 10.1080/21650373.2024.2441463

To link to this article: https://doi.org/10.1080/21650373.2024.2441463

Journal of Sustainable Cement-Based Materials, 2024
http://dx.doi.org/10.1080/21650373.2024.2441463

Preparation of a supplementary cementitious material through synergy CO_2 mineralization of fly ash and carbide slag

Hongzhi Zhang[a], Yingxuan Shao[a], Chuanyi Ma[b], Xianglong Meng[b], Nengdong Jiang[a], Zhi Ge[a]*, Meijun Liang[a,c], Honglei Chang[a] and Branko Šavija[d]

[a]*School of Qilu Transportation, Shandong University, Jinan, PR China;* [b]*Shandong Hi-Speed Group, Jinan, PR China;* [c]*Shandong Hi-Speed Company Ltd., Jinan, PR China;* [d]*Microlab, Faculty of Civil Engineering and Geosciences, Delft University of Technology, Delft, The Netherlands*

(Received 25 December 2023; Accepted 8 December 2024)

A compounded system of fly ash (FA) and carbide slag (CS) was proposed for CO_2 mineralization using the aqueous approach to prepare supplementary cementitious material. Influence of CS dosage on the morphology, particle size distribution, and chemical phases of the carbonation products were characterized. It is found that the mineralization products (calcite) cover on the surface of FA leading to a remarkable synergistic effect in which the CO_2 uptake is improved by about 50%. Furthermore, FA with calcite attached effectively mitigates the set retardation in OPC/FA blends by about 30% and improved the 3- and 28-day compressive strengths by 37.2% and 24.3% respectively due to combined physical and chemical effects. The results indicate that a high-volume cement replacement can be achieved using the carbonated FA produced by the proposed synergy CO_2 mineralization.

Keywords: CO_2 mineralization; fly ash; carbide slag; supplementary cementitious materials; early age performance

1. Introduction

As the most commonly used binder material in construction, annual worldwide production of ordinary Portland cement (OPC) is above 4 billion Mt [1, 2]. It is well known that cement industry is highly energy-intensive and greenhouse gas-emitting because it consumes a great deal of fuel and raw ingredients, e.g. limestone [3, 4]. Approximately, 1.35 billion tons of CO_2 are emitted annually from the OPC production industries alone, accounting for nearly 8–9% of global greenhouse gases emissions [5, 6]. It is estimated that, by the year 2050, the worldwide demand for OPC would increase to nearly 6 billion tones [7]. Reduction of CO_2 emissions from OPC-related activities therefore generates considerable efforts [8, 9].

Coal fly ash (FA) is a by-product of coal burning at coal-fired power plants [10]. The annual output of FA is up to 1000 Mt globally [11]. It is one of the most favorable supplementary cementitious materials (SCMs) and is commonly blended with clinker to make Portland cement or used as a partial replacement for Portland cement in concrete [12, 13]. In practice, replacement levels no more than 20% are commonly used even though FA does provide economic and environmental benefits and improvements in the long-term mechanical properties and durability of concrete [13–15]. This is mainly attributed to the delayed setting and low early age strength when high volume FA is used [16]. Limestone powder has been introduced in the FA/OPC blends. A synergy between FA and limestone powder, which promotes early age strength and hydration [14], resulted in the ternary cements [17]. Additionally, Bentz et al. [18] showed that the fine limestone powder ($<5\,\mu$m) is effective in reducing the initial and final setting time of FA/cement blends. They also concluded that the fineness of the limestone powders dominates their performance as accelerators of reaction and setting. Thongsanitgarn et al. [19] found that the addition of finer limestone powder promotes the heat of hydration both in terms of the rate of heat and the cumulative heat release. The seeding effect of $CaCO_3$ nanoparticles, which accelerates the growth of C–S–H, was reported by Sato and Diallo [20] and Kawashima et al. [21]. As a consequence, such high volume FA concretes resulted in improved early-age and later-age compressive strengths and durability [22]. The later-age strength improvement could be attributed to the promoted pozzolanic reaction of FA [23].

Fine $CaCO_3$ powder can be produced through CO_2 mineralization [24, 25]. In this technique, different polymorphs of $CaCO_3$ nucleate and grow via CO_2 sequestration in a calcium alkoxide solution. By adjusting the liquid-to-solid-ratio, mixing rate of the precursor salts, pH and reaction temperature, calcite, aragonite and vaterite phases can be produced [26–28]. Alkaline solid wastes (e.g. FA, slag blast furnace slag, steel slag, waste gypsum, etc.) may be considered as the most suitable raw materials for CO_2 mineralization due to their high reactivity, intrinsic alkalinity, and availability near industrial sites [29–31]. This generates benefits with respect to CO_2 emission reduction and solid wastes stabilization.

*Corresponding author. Email: zhige@sdu.edu.cn School of Qilu Transportation, Shandong University, Jinan 250002, PR China.

Supplemental data for this article can be accessed online at https://doi.org/10.1080/21650373.2024.2441463.

As one of the most representative alkaline solid wastes, the potential of using FA as a material for mineral CO_2 sequestration generates significant efforts [32]. Both gas–solid and aqueous (liquate–solid) carbonation approach have been applied [28]. The gas–solid approach generally lasts more than a few hours [33, 34]. The efficiency is possibly insufficient for industrial applications. Aqueous carbonation is generally applied to accelerate the CO_2 uptake [35]. However, the carbonation capacity of FA is generally low as the dissoluble calcium content is limited. Attempts have been made to improve the CO_2 sequestration capacity of FA. Increasing the reaction temperature (from 20 to 80 °C) does not seem to significantly increase the carbonation capacity. Ukwattage et al. [36] explained that although the kinetic energy of carbonation reaction is improved, this is partly compromised by rapid formation of a calcite layer on the FA surface. To substantially improve the capacity of CO_2 sequestration, much higher temperature is required [37, 38]. The pressure does influence the reaction process significantly, as the increased pressure promotes CO_2 solubility in liquid thus accelerating the rate of mineralization. However, this does not effectively contribute to the CO_2 uptake capacity [39, 40]. A relatively small solid-to-liquid ratio is an effective way to improve the carbonation efficiency as well as increasing the CO_2 uptake capacity because it can accelerate the release of Ca^{2+} and the CO_2 uptake rate due to a dilution effect [41]. However, the dissolution rate of CO_2 would be reduced with pH of the alkaline solutions. The reported solid-to-liquid ratio in the literature is generally in between 50 and 300 g/L [42, 43].

Based on the literature, it may be possible to substitute OPC with carbonated FA which may perform improved early age properties compared with the OPC/FA blends. However, research on such utilization shows unsatisfactory results [33, 34, 44] as the amount of mineralized carbonate is quite low. To this end, the current study coupled class F FA and calcium carbide residue (a solid waste generated from industrial production of ethylene polyvinyl chloride) for carbonation to produce SCMs. The CO_2 uptake capacity of the binder was measured. The influence of carbonated products on the early age performance (setting time and compressive strength) as well as the mechanism behind were investigated.

2. Materials and methods

2.1. Raw materials

The used raw materials involved P.I. 42.5 OPC, FA (ASTM class F) and carbide slag (CS). OPC was produced by Fushun Cement Corporation (Fushun, China) with a density of 3.11 g/cm^3 and specific surface area (SSA) of 358 m^2/kg. The FA had the Blaine fineness of 341.0 m^2/kg. The chemical composition of the raw materials (measured by X-ray fluorescence (XRF)) is shown in Table 1. The FA has a calcium content of 3.66%. The particle size distributions of the raw materials (measured by a laser particle size analyzer) and shown in Figure 1. The X-ray diffraction (XRD) of raw materials is shown in Figure 2. The crystalline phases identified in the FA include mullite ($3Al_2O_3{\cdot}2SiO_2$), quartz (SiO_2), lime (CaO), anhydrite ($CaSO_4$), and non-crystalline aluminosilicate glass. In CS, the main phase is portlandite.

Table 1. Chemical composition (wt.%).

Component	SiO_2	Al_2O_3	Fe_2O_3	CaO	MgO	SO_3	Others	LOI
Cement	21.82	4.68	3.56	63.43	3.29	2.30	0.92	1.48
FA	56.11	29.60	5.00	3.66	0.77	0.84	4.02	4.05
CS	3.13	1.91	0.44	88.09	0.21	5.77	0.45	24.17

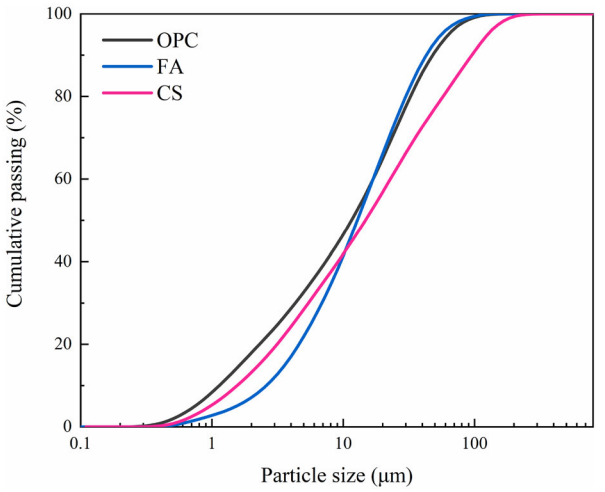

Figure 1. Particle size distribution of raw materials.

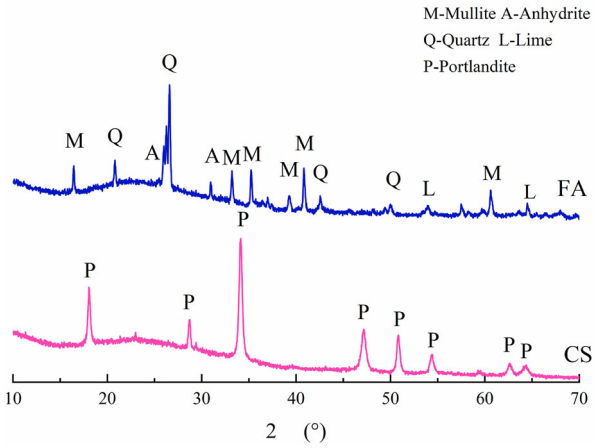

Figure 2. X-ray diffraction (XRD) of raw materials. FA: fly ash; CS: carbide slag.

2.2. Preparation and characterization of carbonated FA

FA and blends of FA and CS were carbonated using the so-called direct aqueous carbonation method as shown in Figure 3 at a room temperature of 20 °C. In terms of the blends, FA was mixed with 5, 10, 15, and 20 wt.% CS to improve the CO_2 uptake capacity and termed as FACS-5, FACS-10, FACS-15, and FACS-20, respectively. The carbonation treated FACS-5, FACS-10, FACS-15, and FACS-20 were termed as CFA, CFACS-5, CFACS-10,

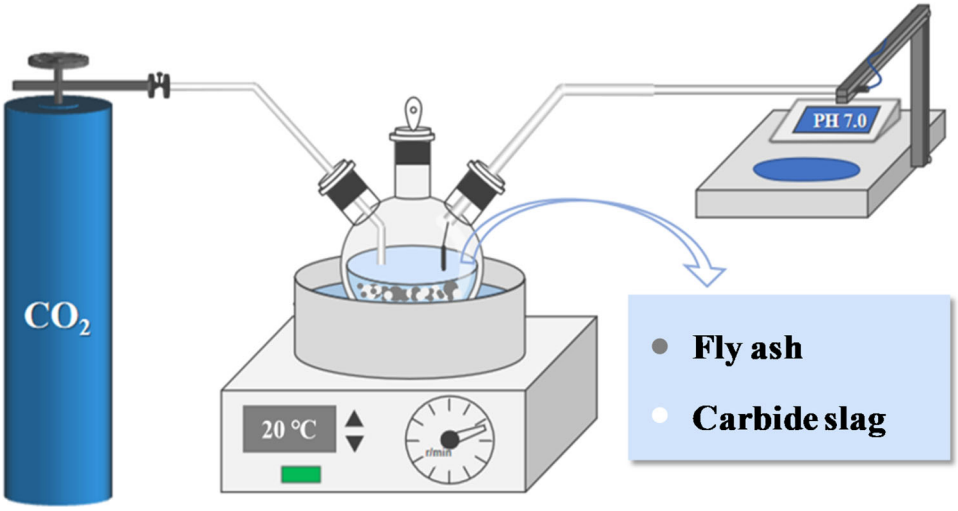

Figure 3. Schematics of the experimental setup used for aqueous carbonation.

CFACS-15, and CFACS-20, respectively. They were collectively referred as carbonated FA in the current study for the sake of simplification. In the direct aqueous carbonation method, solids were first mixed with water in a three-necked flask using a magnetic stirrer switch. The liquid-to-solid ratio of 7.5 was chosen to improve the carbonation efficiency. The effect of different liquid–solid ratios on mineralization efficiency is presented in the supplementary materials. The pH was monitored during mixing and carbonation. Once the pH stabilized, the CO_2 was passed into the slurry at a speed of 0.4 L/min. The pH began to stabilize briefly to 7.0 by 5 min, and a small pH rise occurred after CO_2 injection ceased. After injection of CO_2 briefly for 2–3 times, the pH stabilized at 7.0. The hole process was around 6 min. The slurries were then filtered using a 0.1 μm filter and vacuum dried for 24 h at temperature of 105 °C.

The particle size distribution of carbonated FAs was measured by a laser particle size analyzer using the fluid module which has a measurement range of 0.02–2000 μm. Scanning electron microscope (SEM) under second electron (SE) mode was used to observe the morphology of FA particles. Carbonated particles were ground and sieved for the XRD, Fourier transform infrared spectroscopy (FTIR) and thermogravimetric analysis (TGA) tests. The XRD spectra of carbonated FA particles were obtained by an X-ray diffractometer with Cu-Kα radiation and the samples were scanned in the range of $5° \leq 2\theta \leq 90°$ with a step rate of 2°/min and scanning step of 0.02°/min. FTIR measurement was conducted using the conventional KBr disc method (1.0 mg of sample to 300.0 mg of KBr). Frequencies were scanned across a range of 4000–400 cm^{-1}. TGA was performed using about 10 mg of the FA powders. During the measurement, samples were heated from 20 to 900 °C at rate of 10 °C/min in nitrogen atmosphere.

2.3. Testing of blended OPC/FA pastes

The blended cement mixes consist of 70% OPC and 30% FAs by weight. The mix proportion is given in Table 2.

Table 2. Mix proportions of blended cement pastes.

Mixes	OPC content (wt.%)	FA type	FA content (wt.%)	w/b
OPC	100	–	0	0.40
OPC/FA	70	FA	30	0.40
OPC/CFA	70	CFA	30	0.40
OPC/CFACS-5	70	CFACS-5	30	0.40
OPC/CFACS-10	70	CFACS-10	30	0.40
OPC/CFACS-15	70	CFACS-15	30	0.40
OPC/CFACS-20	70	CFACS-20	30	0.40

The water-to-binder (w/b) ratio was 0.4 for all the mixes. Pure OPC paste was used as reference.

Water requirement of normal consistency was tested by the Vicat apparatus according to GB/T 1346. Setting times of pastes were determined using the Vicat needle. The initial and final setting time are defined as the elapsed time required for the penetration depth of Vicat needle at needle penetrate 36 ± 1 mm and 0.5 mm, respectively.

Heat of hydration was measured by isothermal calorimetry at ambient temperature (20 °C). The heat flow was recorded every 60 s up to 72 h. SEM and XRD analyses were performed out on the hydrated pastes at the age of 3 days and 28 days to investigate the influence of carbonated FAs on the microstructure and hydration products. The amount of hydrated water and portlandite at 28 days was measured using TGA. For the sample preparation, the fresh paste was first mixed using a Hobart mixer and then cast in a plastic cylindrical mold with 25 mm diameter and 57 mm height. Afterwards, the cylinder was rotated at a speed of 30 rpm at room temperature (20 °C) for 24 h to minimize bleeding, and subsequently placed in the standard curing room ($T = 20 \pm 2$ °C, RH $\geq$ 95%) in sealed conditions until the test age. The hydration of the hydrated paste was arrested by solvent exchange method using isopropanol [45]. For the XRD and TGA test, paste was ground into powder and sieved through 320 mesh. Before the test, the samples were stored in a vacuum oven with 40 °C for 24 h to evaporate the isopropanol.

Mortars were prepared for the strength activity index (SAI) measurement following the Chinese Standard GB/T 1596-2017. The water-to-binder ratio and sand-to-binder ratio were 1/2 and 1/3, respectively. After mixing, the materials were cast in cubic mold with size of 40 mm and placed in the room with a temperature of 20 ± 2 °C under sealed condition for one day. They were then demolded and cured in lime-saturated water until the age of 3 days and 28 days. Compressive strength measurement was then carried out according to Chinese Standard GB/T 17671. A loading rate of 0.6 kN/s was used. For each mix, six specimens were tested and the average value was used for calculating the SAI.

3. Results and discussion

3.1. Carbonated FA

3.1.1. Morphology

Morphology of FAs before and after CO_2 mineralization is shown in Figure 4. As it can be seen from Figure 4(a), FAs are spherical particles. Due to the low calcium content, the calcium carbonate particles are small and dispersed on the CFA surface (see Figure 4(b)). With addition of CS and leaching of Ca^{2+}, the calcium concentration of the liquid increases, generating larger calcium carbonate particles with a cubic shape (see Figure 4(c–f)). These particles cover on the FA surface (called 'ectopic

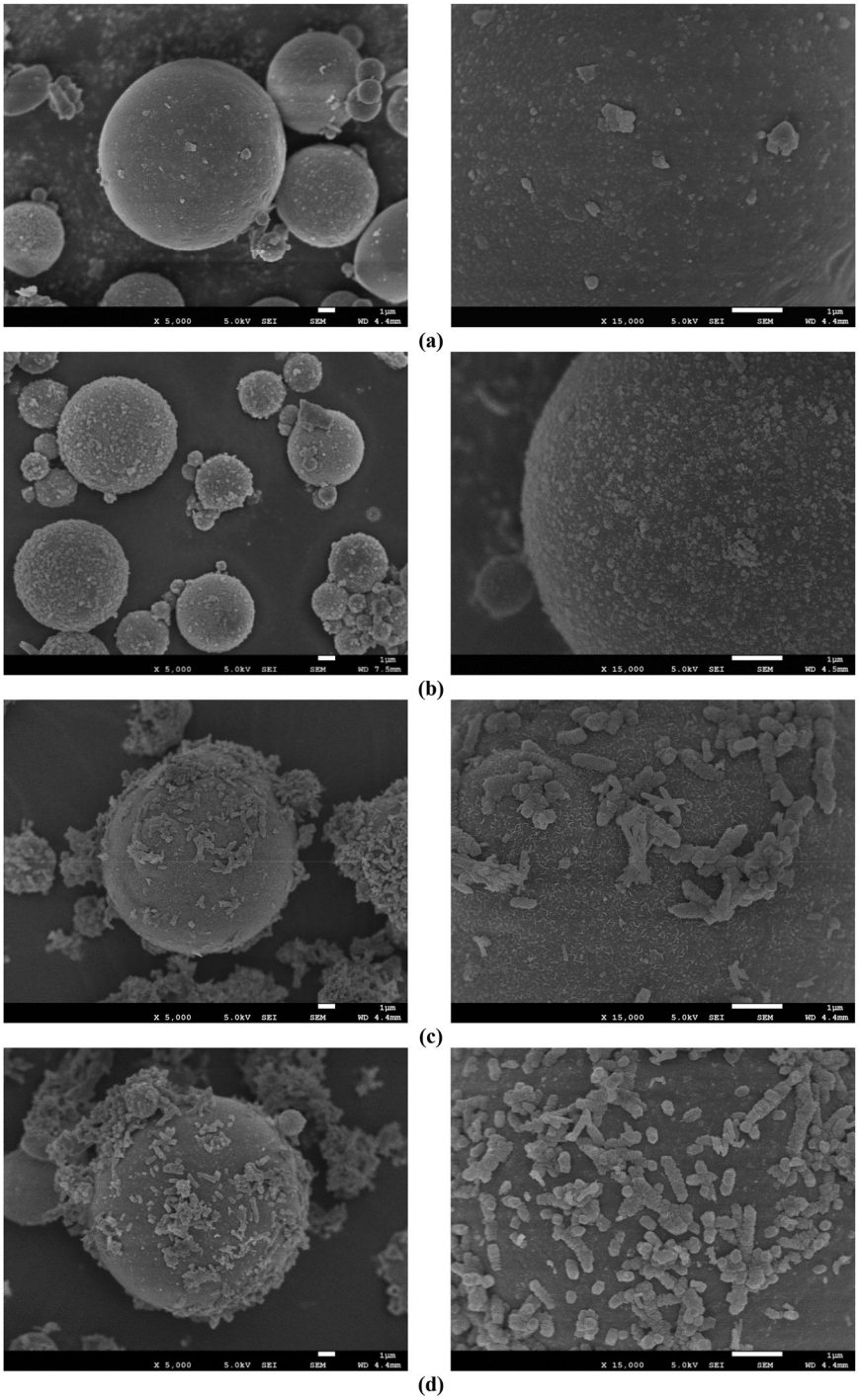

Figure 4. SEM images of carbonated and non-carbonated FA: (a) FA; (b) CFA; (c) CFACS-5; (d) CFACS-10; (e) CFACS-15; (f) CFACS-20; (g) SEM-EDS results of carbonated FA.

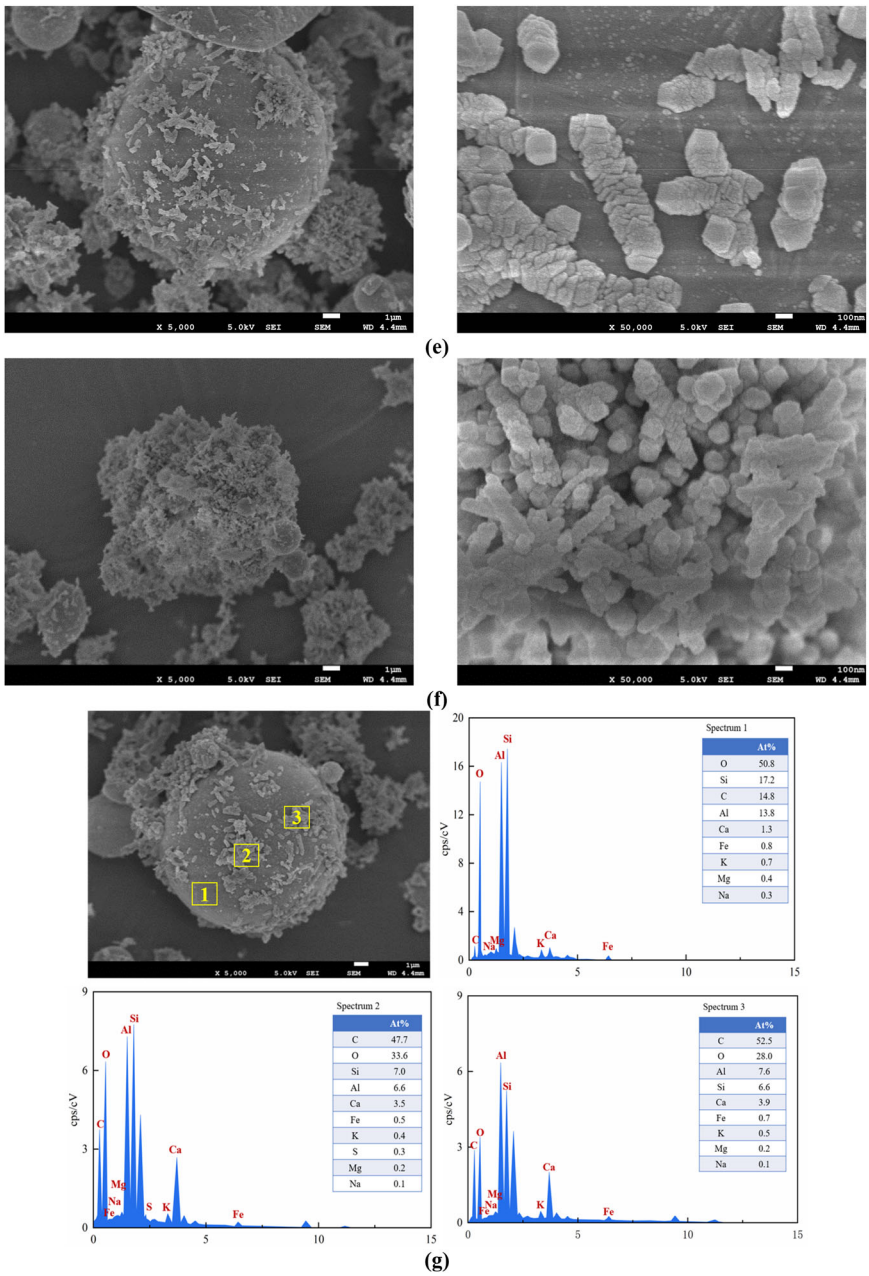

Figure 4. Continued.

cover') and further agglomerate and form clusters. The amount of C, O, and Ca increased significantly when points 2 and 3 were struck on particles dispersed on the CFA surface compared to point 1, indicating $CaCO_3$ was present (see Figure 4(g)). This is in in accordance with Ma et al. [46]. Because during the mineralization, an alkaline environment leads to a positive zeta potential of CS and a negative zeta potential of FA. Consequently, FA particles preferentially absorb Ca^{2+} through the electrostatic attraction force. Once the nuclei are formed, a large amount of $CaCO_3$ grows.

3.1.2. *Particle size distribution*

FA displays a unimodal particle size distribution [47] and consists of a major population with grain sizes around 20 μm (Figure 5). After carbonation, the SSA increases by

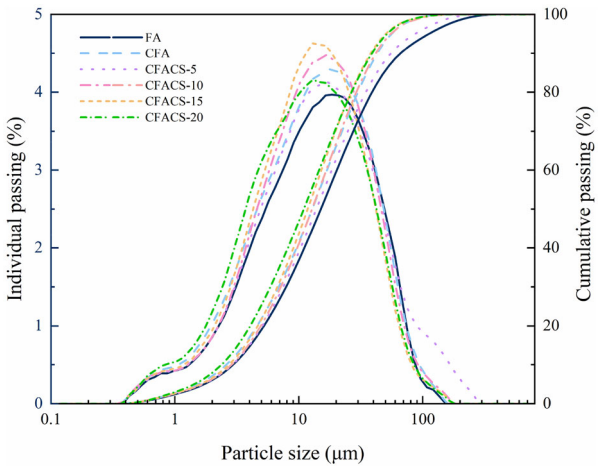

Figure 5. Particle size distribution of LFA before and after carbonation.

Table 3. Specific surface area and particle size distribution of FA before and after carbonation.

Sample	SSA (m^2/kg)	Particle size distribution (%)		
		<5 μm	5–20 μm	>20 μm
FA	341.0	19.02	40.54	40.44
CFA	353.6	19.66	43.15	37.19
CFACS-5	369.4	20.27	46.60	33.13
CFACS-10	384.1	21.71	47.72	30.57
CFACS-15	383.2	21.86	48.52	29.62
CFACS-20	420.0	25.40	45.50	29.10

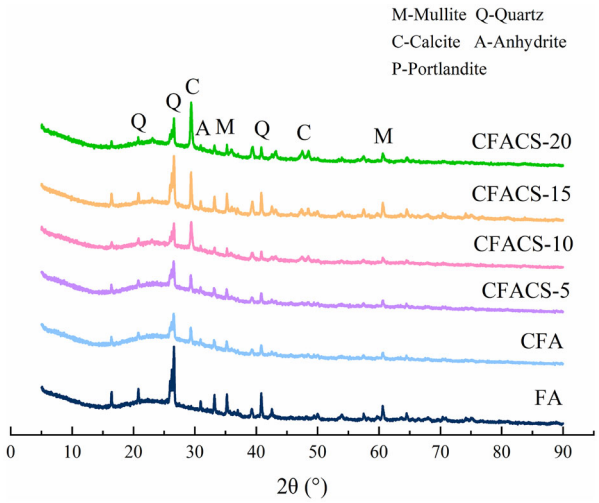

Figure 6. XRD patterns of un- and carbonated FA.

3.7% for CFA and 23.2% for CFACS-20. The amount of fine (<5 μm) and medium size (5–20 μm) particles increase and large (>20 μm) particles decrease. This trend becomes more remarkable with CS amount increasing. Similar observation has been reported in Shao et al. [48]. The raise of fine particles can be attributed the agglomeration of $CaCO_3$ in the solution. Furthermore, the leaching of Ca^{2+} and Mg^{2+} leads to the reduction of particle size. The adsorption and precipitation of carbonate solids on the surface of FA lead to the volume percentage increment of medium size. However, different trends are observed for Chen et al. and Jaschik et al. [34, 49] as different carbonation conditions are applied (Table 3).

3.1.3. XRD and FTIR

The XRD patterns of original and carbonated FAs are compared in Figure 6. It shows that the mineralization product mainly consists of calcite. With the addition of CS, significantly enhanced calcite diffraction peaks are observed for CFACS-15 and CFACS-20.

Findings from the XRD analysis are supported by the FTIR results (see Figure 7). The absorption bands of 460 cm^{-1}, 560 cm^{-1}, and 1096 cm^{-1}, which appear in all FAs, correspond to the Si–O stretching vibration, indicating the presence of quartz. The CO_3^{2-} bending (v_2, 875 cm^{-1}) band and C–O bending (v_3, 1420 cm^{-1}) are assigned to the peak characteristic of calcite [50]. All carbonated FAs display an additional absorption band at 1793–1799 cm^{-1}, which indicates the presence of calcite

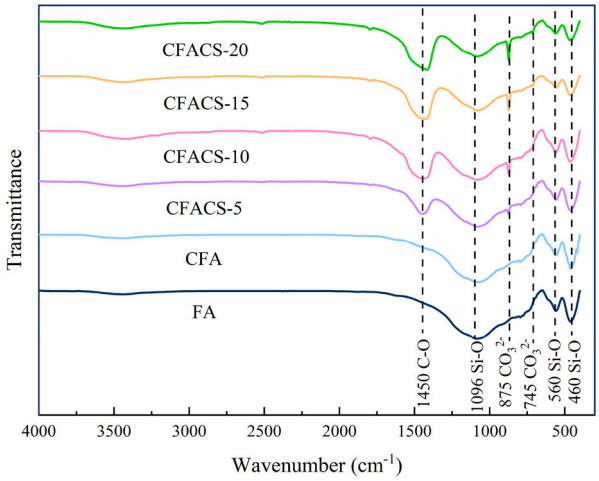

Figure 7. FTIR spectra of un- and carbonated FA.

[51]. In addition, the absorption band of 745 cm^{-1} indicates the presence of vaterite [52], which is not detected by XRD due to its low content. Unlike the mineralization system using hydrated cement paste powder or steel slag [53–55], no silica gel nor calcium silicate mineral is observed to be generated during the mineralization process using FA and CS. This can be attributed to the fact that the hydration process of FA is quite slow [14, 15] and the mineralization process lasts for only 6 min which limits the production of silica gel and calcium silicate mineral.

3.1.4. TGA

TGA results are presented in Figure 8. Mass loss peak at 550–900 °C is observed in all carbonated FAs, which is attributed to the decomposition of $CaCO_3$ [56]. This is consistent with the observations in XRD and FTIR. Clearly, addition of CS leads to the $CaCO_3$ decomposition peak shifting to higher temperature, indicating that a higher crystallinity is achieved [57]. The CO_2 uptake and carbonation efficiency can be calculated based on TGA results as:

$$w(CO_2) = \frac{\Delta m_{550-900\ ^\circ C}}{m_0} \times 100\% \quad (1)$$

$$CO_{2\,uptake} = 1000 \times \frac{w(CO_2)}{1 - w(CO_2)} \quad (2)$$

$$\zeta CaO(\%) = \frac{\frac{w(CO_2)}{100-w(CO_2)} \times \frac{1}{MW_{CO_2}}}{Ca_{total}/MW_{Ca}} = \frac{\frac{w(CO_2)}{100-w(CO_2)} \times \frac{1}{MW_{CO_2}}}{CaO_{total}/MW_{CaO}} \quad (3)$$

where $\Delta m_{540-800\ ^\circ C}$ is the weight loss between 550 and 900 °C for the carbonated sample, m_0 is the initial mass of samples, $w(CO_2)$ is the mass fraction of CO_2 in the carbonated sample, MW_{CO2}, MW_{Ca}, and MW_{CaO} are the molecular weight of the CO_2, Ca, and CaO (g/mol), Ca_{total} and CaO_{total} are the percent weight fraction determined by the XRF.

The results are shown in Table 4. Carbonation efficiency takes into account the calcium in all Ca-bearing minerals of the CS and FA (i.e. anhydrite, free lime, portlandite, and Ca-silicates) [51]. FA has a quite low

carbonation efficiency (17.0%). CS has much higher carbonation efficiency than FA as it contains mainly the soluble portlandite while the calcium in FA. The carbonation efficiency is significantly increased when CS and FA is coupled for the carbonation. Notably, the carbonation efficiency of CFACS-15 and CFACS-20 is even higher than pure CS.

Supposing the carbonation process of CS and FA is independent, the theoretical CO_2 uptake of the mixed binders (FA and CS) is calculated. Clearly, the measured CO_2 uptake is much higher than the theoretical one. This means there exists a synergistic effect of FAs coupled with CS for mineralization of CO_2. This can be attributed to the fact that, as shown in Figure 5, FA offers a large amount of surface for $CaCO_3$ to grow on and leaves more exposed sites of CS for Ca^{2+} dissolution [46]. Furthermore, CS contains a large number of portlandite which can act as alkali activator to promote the Ca^{2+} dissolution from FA [36]. A synergistic effect ratio is defined as the ratio between real measured and theoretical calculated CO_2 uptake amounts. In general, it increases with the CS amount and reaches 1.25 for CFACS-15. The CO_2 uptake improvement is much higher than the other techniques, e.g. increasing temperature and pressure [36, 37, 39].

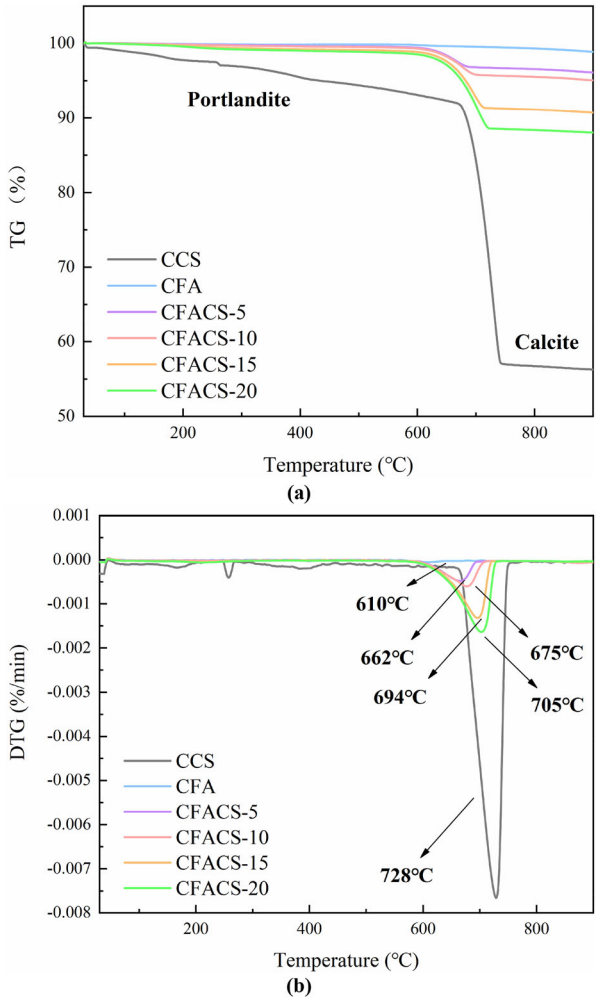

Figure 8. TG–DTG curves of FA before and after carbonation: (a) TG and (b) DTG.

3.2. *Blended OPC/FA mixes*

3.2.1. *Workability and setting time*

The water demand of normal consistency and setting times of the mixes are given in Table 5. Addition of FAs slightly increases the water demand. After carbonation, the water demand is further increased as the mineralization results in much higher SSA of FA particles [58].

The initial and final setting times for OPC are 115 and 185 min, respectively. As expected, addition of FA in cement significantly delays the setting. This is because the FA particles mainly work as a diluent material at early ages, not participating in the flocculation and setting processes [59].

Carbonation treatment can effectively mitigate the set retardation in OPC/FA blends. However, the reduction of setting time is not significant for CFA, as limited calcite is formed. This is enhanced by addition of CS during carbonation. Clearly, compared with FA, CFACS-10 leads to 17.8% and 19.7% reduction in the initial and final setting times. The reduction is more significant for CFACS-20: 29.3% and 32.8% for initial and final setting times,

Table 5. Workability and setting times of OPC/FA blends.

Mixes	Water requirement of normal consistency (%)	Setting time (±10 min)	
		Initial	Final
OPC	26.0	115	185
OPC/FA	26.6	225	305
OPC/CFA	27.6	205	295
OPC/CFACS-5	27.8	200	270
OPC/CFACS-10	28.2	185	245
OPC/CFACS-15	29.5	170	235
OPC/CFACS-20	30.0	145	205

Table 4. CO_2 uptake and carbonation efficiency of CS and FA after carbonation.

Sample	Carbonation efficiency (%)	Measured CO_2 uptake ($kg \cdot t^{-1}$)	Theoretical CO_2 uptake ($kg \cdot t^{-1}$)	Synergistic effect ratio
CCS	68.9	477	–	–
CFA	17.0	5	–	–
CFACS-5	57.6	36	33.6	1.07
CFACS-10	63.8	58	52.2	1.11
CFACS-15	66.5	95	75.8	1.25
CFACS-20	72.0	120	99.4	1.21

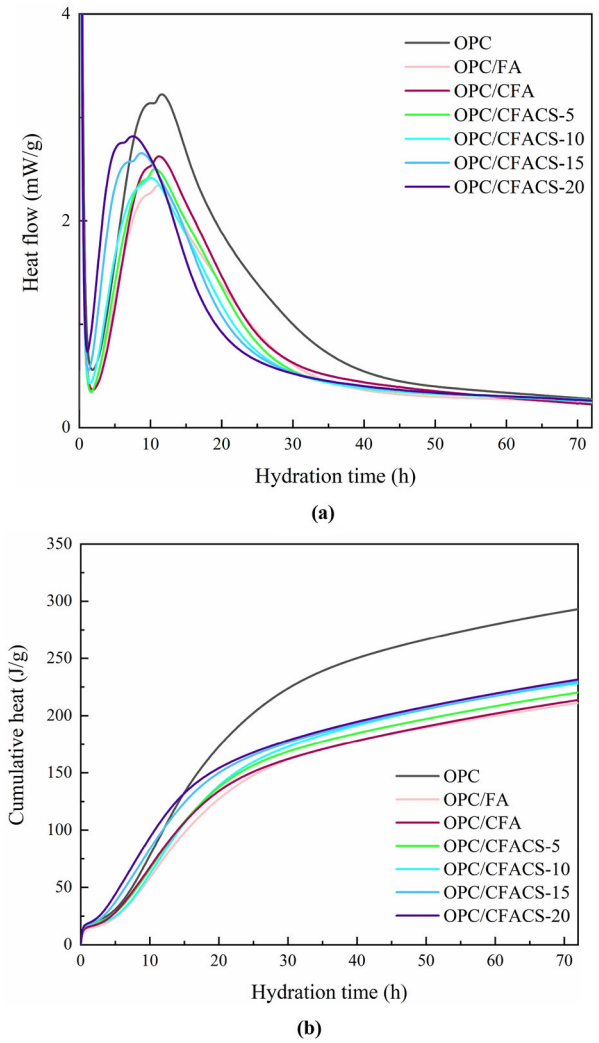

Figure 9. Hydration heat of cement paste: (a) heat flow curves and (b) cumulative heat.

respectively. This can be attributed to the mineralized calcium carbonate during carbonation treatment. It has been reported that the small calcium carbonate particles can stick to larger cement particles and provide seeding sites for the hydration products of the cement, which facilitates the formation of percolated solid backbone [60, 61].

3.2.2. *Hydration heat*

The isothermal calorimetry heat profiles show the heat of hydration per gram of the binder evolved during the first 72 h at a constant w/b ratio of 0.4 (Figure 9). OPC is given as reference. The hydration process can be separated into four stages: initial reaction period, induction period, acceleration period, and retardation period [62]. Two humps of the main hydration peak are observed in Figure 9(a). The first is caused by the hydration of calcium silicates, mainly tricalcium silicates (C_3S) and the second corresponds to renewed reaction of the aluminate phases in which further hydration of tricalcium aluminate (C_3A) proceeds [63]. Substitution of OPC with FA leads to a delay of hydration heat development. On the other hand, when CFACS-10 and CFACS-20 are used, isothermal calorimetry curve is shifted to earlier times with respect to pure OPC. This

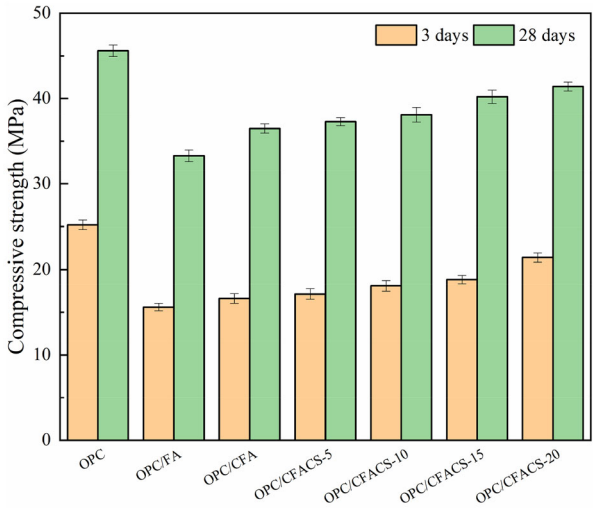

Figure 10. Compressive strength of cement mortar mixed with FA.

indicates that the presence of calcium carbonate generated in carbonated FA reduces the induction period and accelerates the cement hydration. Similar trend has been observed in a ternary Portland cements containing fine limestone powder and FA [19]. Furthermore, the height of the main hydration peaks is associated with the amount of mineralized calcium carbonate in FA: higher mineralized calcium carbonate content corresponds to stronger exothermic peaks. This trend also applies for the measured cumulative heat of the 72 h hydration (see Figure 9(b)). At least two mechanisms are involved for the influence of mineralized calcium carbonate on the early age hydration of these blended cement pastes. The first can be attributed to the filler effect of these small particles (<5 μm) providing additional surfaces for the nucleation and growth of hydration products [64]. The second mechanism may be related with the enriched calcium ion content in the pore solution due to the dissolution of calcium carbonate [65].

As shown in Figure 9(b), replacement of OPC by FA results in a reduction in the total released heat, due to the slow reaction of FA and the cement dilution effect. The total heat of OPC/FA and OPC/CFA released up to 72 h is much lower than OPC/CFACS-series. The trend observed in the emitted cumulative heat is the same as the compressive strength of their equivalent mortar (Figure 10).

3.2.3. *XRD*

The principal hydration products in all blends are similar to net OPC (Figure 11). Three major crystalline phases identified are portlandite, calcium carbonate, and unreacted tricalcium silicate. Calcite peaks are more evident in OPC/CFACS-15 and OPC/CFACS-20, as more calcite is initially incorporated in these mixes. Due to the ongoing hydration, the diffraction peak of tricalcium silicate is reduced at 28 days.

The XRD patterns of the hydrated cement pastes at low angles are compared in Figure 12. At three days, ettringite (9.1° 2θ) and ferrite (12.2° 2θ) are observed in all mixes. Monosulfate (Ms 9.8° 2θ), which is a result of the reaction between remaining aluminates and ettringite

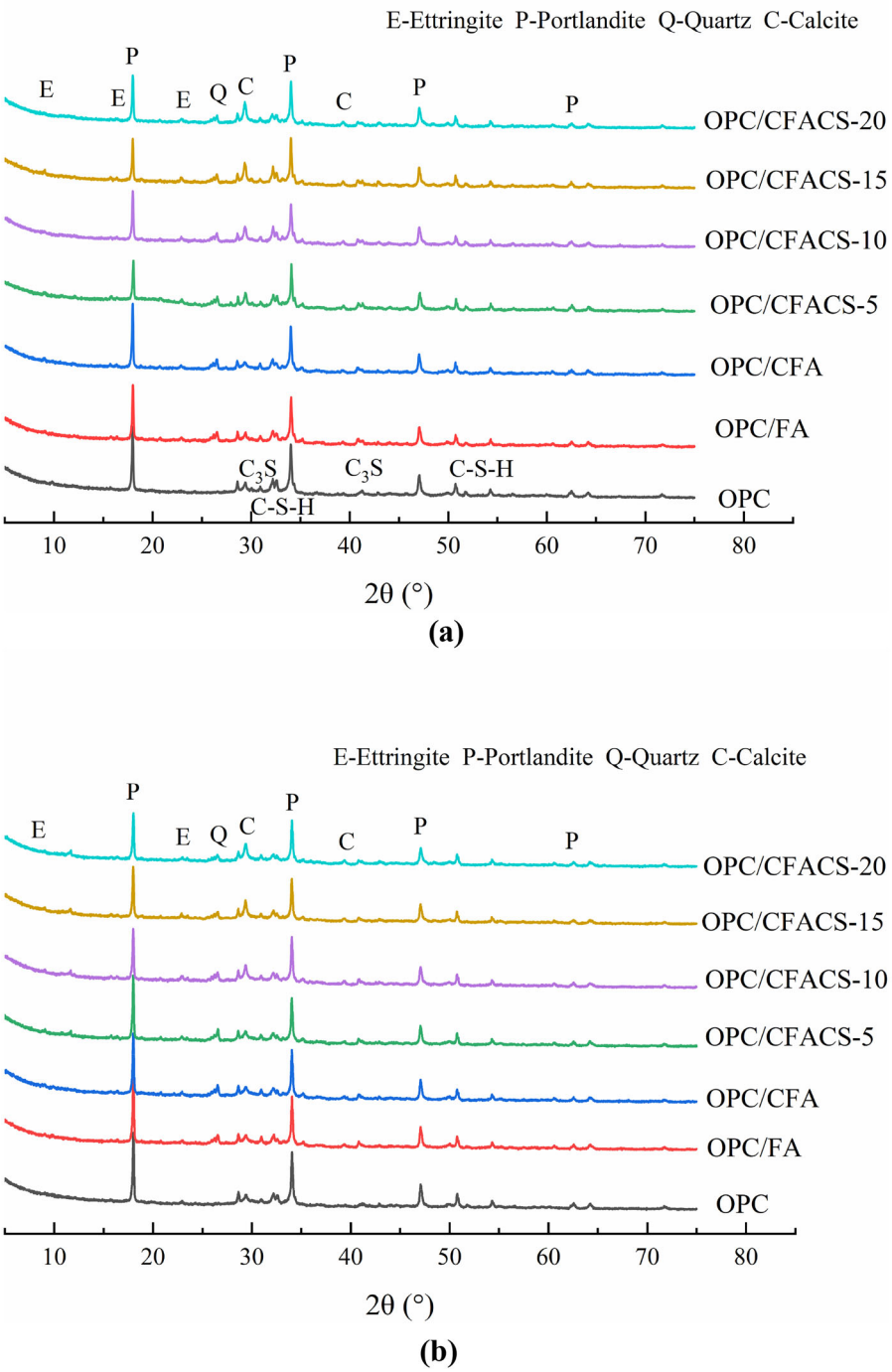

Figure 11. XRD patterns for the hydrated cement pastes at the age of: (a) three days and (b) 28 days.

when gypsum is consumed [66], is found in pure OPC, OPC/FA, and OPC/CFA. In the presence of $CaCO_3$, this reaction is inhibited [67], thus no Ms appears in OPC/CFACS-series. Instead, mono- and hemicarbonate (Mc at 11.7° 2θ and Hc at 10.8° 2θ) are found [14, 68]. The exception for OPC/CFA is due to the limited $CaCO_3$ amount. Additionally, for OPC and OPC/FA system, there is also a broad peak between Ms and Hc, which may be related to the carbonate and sulfate containing hydroxy-AFm (AFm*) [14]. At 28 days, AFm* remains.

At 28 days, the reduction of ettringite and increase of Ms in OPC/FA and OPC/CFA are observed due to the on-going hydration. In terms of OPC/CFACS-series, the differential peak of ettringite remains [68]. Furthermore, with hydration going on, Hc peak decreases in OPC/CFACS-series, whereas the peak of Mc increases. This is because Mc is thermodynamically more stable than Hc [69, 70] and Hc would transform into Mc. However, at 28 days, Hc still remains in the system as this process is quite slow. This observation is in accordance with references [14, 68] in which Hc is presented until 90 days.

3.2.4. TGA

The weight loss in hydrated blended cement paste at 28 days on heating is compared in Figure 13. Three peaks can be clearly seen on the DTG curves. The first peak is

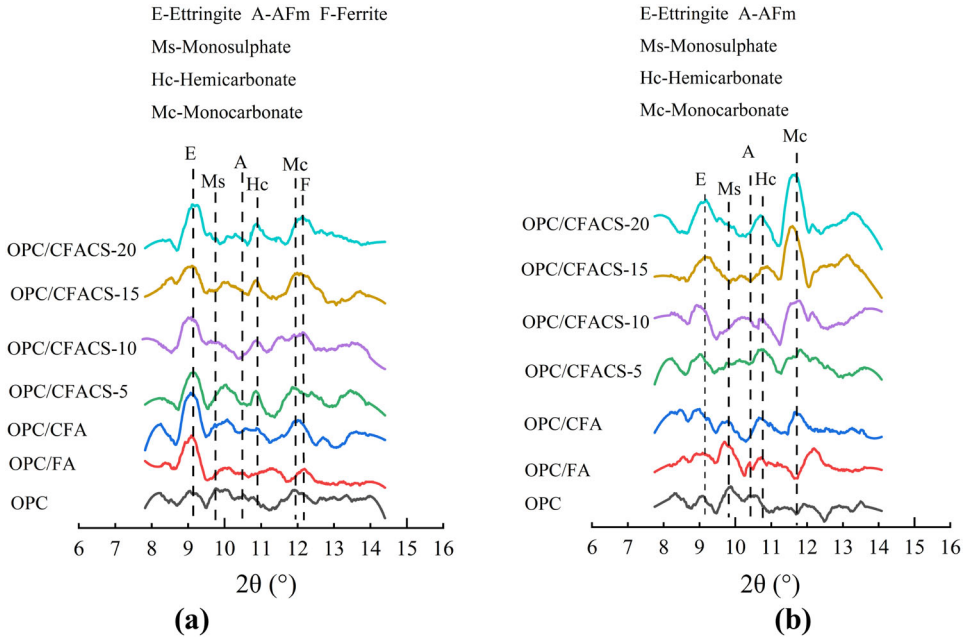

Figure 12. XRD patterns of low angles for the hydrated cement pastes at the age of: (a) three days and (b) 28 days.

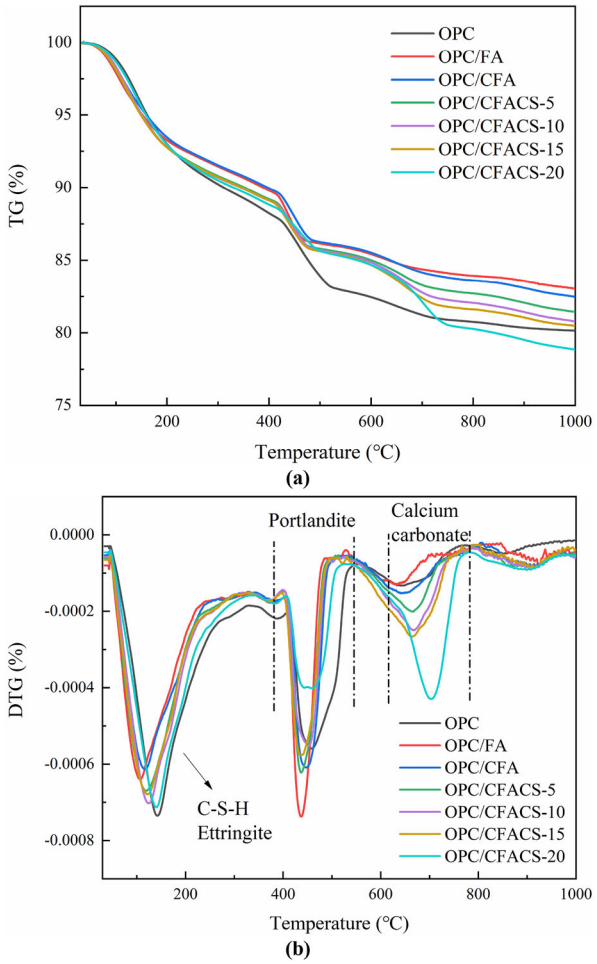

Figure 13. Weight loss and derivative weight loss curves for cement paste at 28 days.

in between 30 and 200 °C, and is generated by the decomposition of ettringite, monosulfate hydrate, and C–S–H gel [71].

The second peak occurs between 350 and 550 °C, which is attributed to the decomposition of portlandite [72]. Decomposition of calcium carbonate leads to the third peak in the range of 650 and 800 °C [56]. The weight loss between 650 and 700 °C indicates the presence of amorphous or poorly crystalline calcium carbonate that can decompose at lower temperatures. This can be attributed to the natural carbonation process during the curing and sample preparation process in which vaterite and aragonite are formed. These polymorphs of calcium carbonate possess lower decomposition temperature compared with calcite due to the lower thermodynamic stability [73]. The intensity of the weight loss peak correlates with the calcite content mineralized by the FA, showing that some of the added calcium carbonate is still stable in the matrix and does not participate in the reaction.

The hydrate water and portlandite content was calculated using the weight loss between 40–550 °C and 350–550 °C, respectively:

$$H = \frac{\Delta m_{40-500^\circ C}}{m_{500^\circ C}} \tag{4}$$

$$CH = \frac{\Delta m_{350-500^\circ C}}{m_0} \times \frac{74}{18} \tag{5}$$

where $\Delta m_{40-500\,^\circ C}$ is the weight loss between 40 and 500 °C in the sample, m_0 is the initial mass of samples, $\Delta m_{350-550\,^\circ C}$ is the weight loss between 350 and 500 °C in the sample.

The content of hydrate water and portlandite in the hydrated pure OPC and blended cement pastes are compared in Table 6. The hydrated water increases with the mineralized calcium carbonate content in FA. 5.6% hydrated water increment is observed for CFACS-20 compared with FA. Similar observation has been reported in a ternary system containing OPC, FA, and limestone powder [74].

Substitution of cement using FA leads to the reduction of portlandite content due to the diluted cement content as well as the pozzolanic reaction of FA [75]. After carbonation treatment, the portlandite content is significantly reduced in the hydrated blends which is a sign for the improved binder reactivity [76]. In terms of OPC/FA, the portlandite content reduces with the incorporated calcite content which controls the available carbonates in the pore solution and governs the formation of Hc in which portlandite is consumed [77].

3.2.5. MIP

Figure 14 shows the pore size distribution of OPC/FA, OPC/CFA, and OPC/CFACS-20 at 28 days. Porosity and threshold pore diameter are calculated and listed in Table 7. Compared with OPC/FA, the porosity of OPC/CFA and OPC/CFACS-20 at 28 days decreased by 8.9% and 17.5%, respectively. Similar trend is observed for the threshold pore diameter.

Based on the Zhao [78], the pore size can be divided into four categories: <20 nm, 20–50 nm, 50–200 nm, and >200 nm, representing harmless pores, less harmful pores, harmful pores, and multi-harmful pores. As can be seen in Figure 15, compared with OPC/FA, the proportion of harmful pores in OPC/CFACS-20 decreases by 31.9%. Apparently, CFACS-20 significantly reduces the porosity and refines the pore structure, thus leading to a higher compressive strength.

3.2.6. Compressive strength

Compressive strengths of mortars cured for 3 and 28 days are shown in Figure 10. Addition of 30% non-carbonated FA significantly reduces the compressive strength. The SAI is calculated as the ratio between the compressive of blended OPC/FA mortar and reference net OPC mortar. Clearly, for all FAs, the 28-day SAI is higher than the three-day one as the pozzolanic reaction of FA mainly occurs at late stage and the FA is relatively inert at the early stage [79]. Compared with FA blended cement, the early strength improvement by using CFACS-series can be attributed to the following factors: calcite in CFACS-20 can provide active nucleation sites for hydrates and participate in the formation of Mc and Hc. Ettringite is therefore retained, which has larger volume than Ms and AFm [80]. In addition, CFACS-series can improve the amount and density of outer hydration products. Therefore, harmful and multi-harmful pores are transformed into less harmful

Table 6. Content of hydrate water and portlandite in cement paste.

Mixes	Hydrate water (wt.%)	Portlandite (wt.%)
OPC	17.11	26.37
OPC/FA	13.98	19.68
OPC/CFA	14.07	19.32
OPC/CFACS-5	14.15	19.30
OPC/CFACS-10	14.60	19.14
OPC/CFACS-15	14.72	18.66
OPC/CFACS-20	14.76	18.51

Table 7. Pore structure parameters of cement pastes.

Samples	Age (day)	Porosity (%)	Threshold pore diameter (nm)
OPC	28	21.07	26.39
OPC/FA		30.00	56.71
OPC/CFA		27.32	55.26
OPC/CFACS-20		24.75	45.11

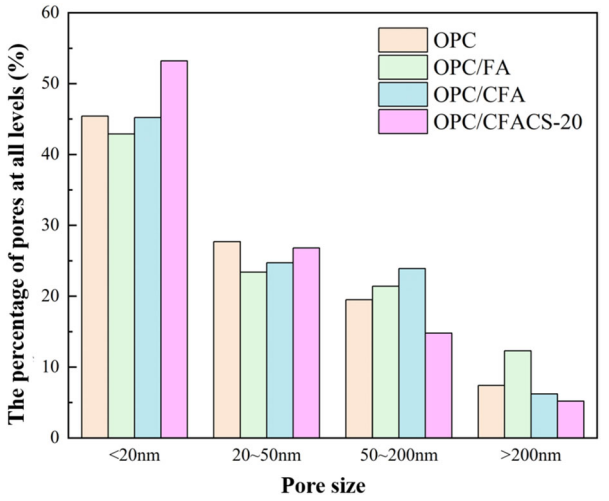

Figure 15. Pore diameter distribution of cement pastes at 28 days.

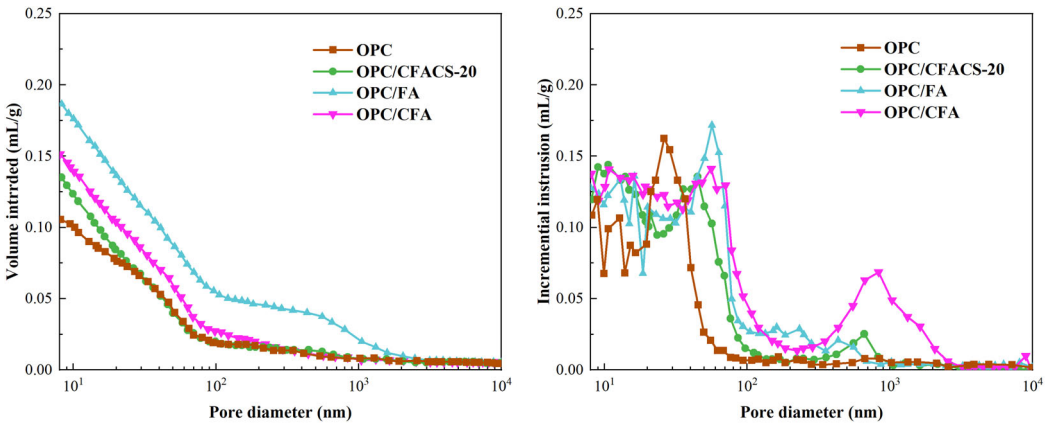

Figure 14. MIP results of cement pastes.

or harmless pores, optimizing the pore structure and the densify microstructure.

It is evident that the carbonation treatment increases the SAI of FAs. SAI increases remarkably with the mineralized calcium carbonate content in FA, suggesting that the mineralized calcium carbonate is beneficial to the compressive strength gain of the blends. With respect to CFACS-20, the 3-day and 28-day SAIs are 84.9% and 90.8%, which are 37.2% and 24.3% higher than FA, respectively. This is much higher compared with the available data in the literature [34, 44]. The improvements in both SAI and setting time could allow the use of high-volume FA mixes with sufficient engineering properties (Table 8).

3.2.7. SEM

The microstructure of the hydrated blended cement pastes at three days is shown in Figure 16. C–S–H gel and calcium hydroxide can be clearly seen in each mix, but the compaction degree of the hydration products varies. Furthermore, spherical FA particles are observed in all mixes, indicating that the FA plays a major role in filling and acts as a micro-aggregate at early ages. For OPC/CFACS-10 and OPC/CFACS-20, more ettringite is observed which is consistent with the above analysis.

The microstructure of hardened cement pastes at 28 days is shown in Figure 17. It is much denser than at three days. The hydration products are deposited on the FA particles and grow with ongoing hydration. FA particles become honeycombed due to the pozzolanic reaction [81, 82]. Additionally, it is evident that after carbonation treatment, the surface of FA dissolves more indicating a higher hydration degree. The hydration degree seems to increase with amount of calcium carbonate formed during carbonation. The calcium carbonate can interact with aluminates from FA after a few days. The formed carboaluminates contribute to the space-filling process in the capillary region and, thereby, to higher compressive strength.

Table 8. Strength activity index of FAs.

	Strength activity index (SAI) (%)	
FA type	3 days	28 days
OPC/FA	61.9	73.0
OPC/CFA	65.9	80.0
OPC/CFACS-5	68.0	81.8
OPC/CFACS-10	71.8	83.6
OPC/CFACS-15	74.8	88.2
OPC/CFACS-20	84.9	90.8

4. Conclusions

This work explored the feasibility of using FA coupled with CS for CO_2 mineralization to enhance its CO_2 sequestration capacity and performance as SCMs. Binders with different FA and CS amounts were carbonated at atmospheric temperature and normal pressure using the

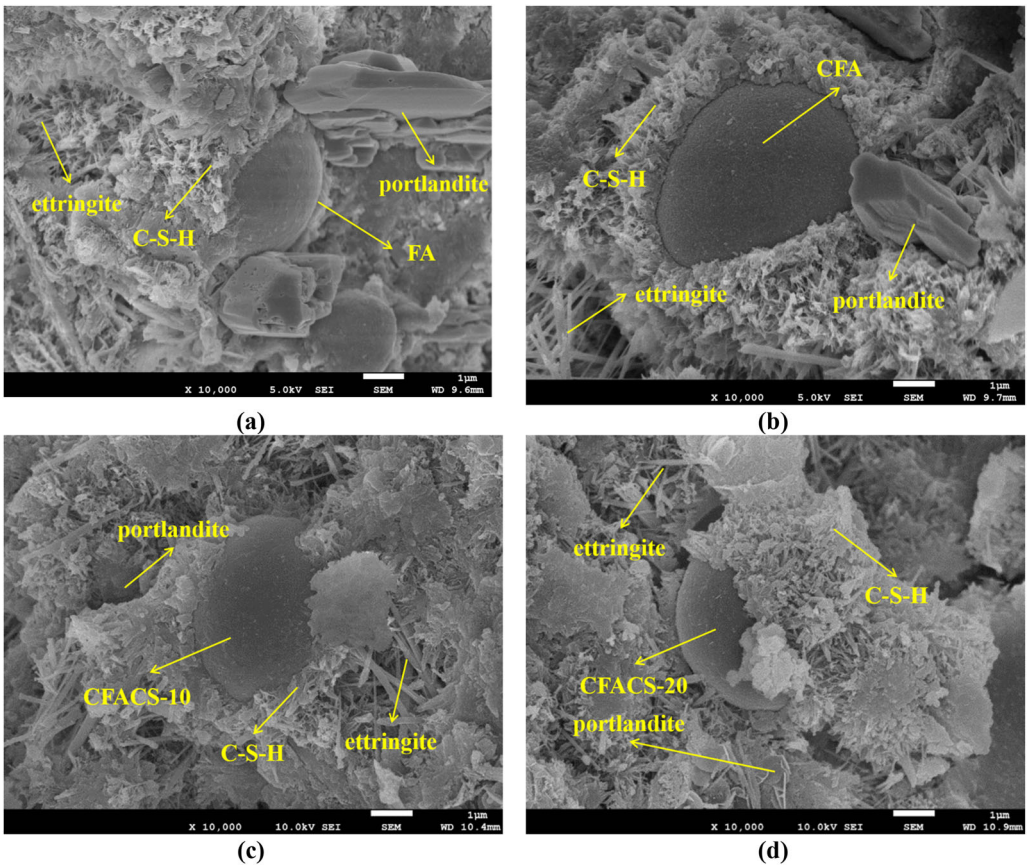

Figure 16. SEM images of cement pastes after three days of hydration: (a) OPC/LFA; (b) OPC/CLFA; (c) OPC/CLCS-10 and (d) OPC/CLCS-20.

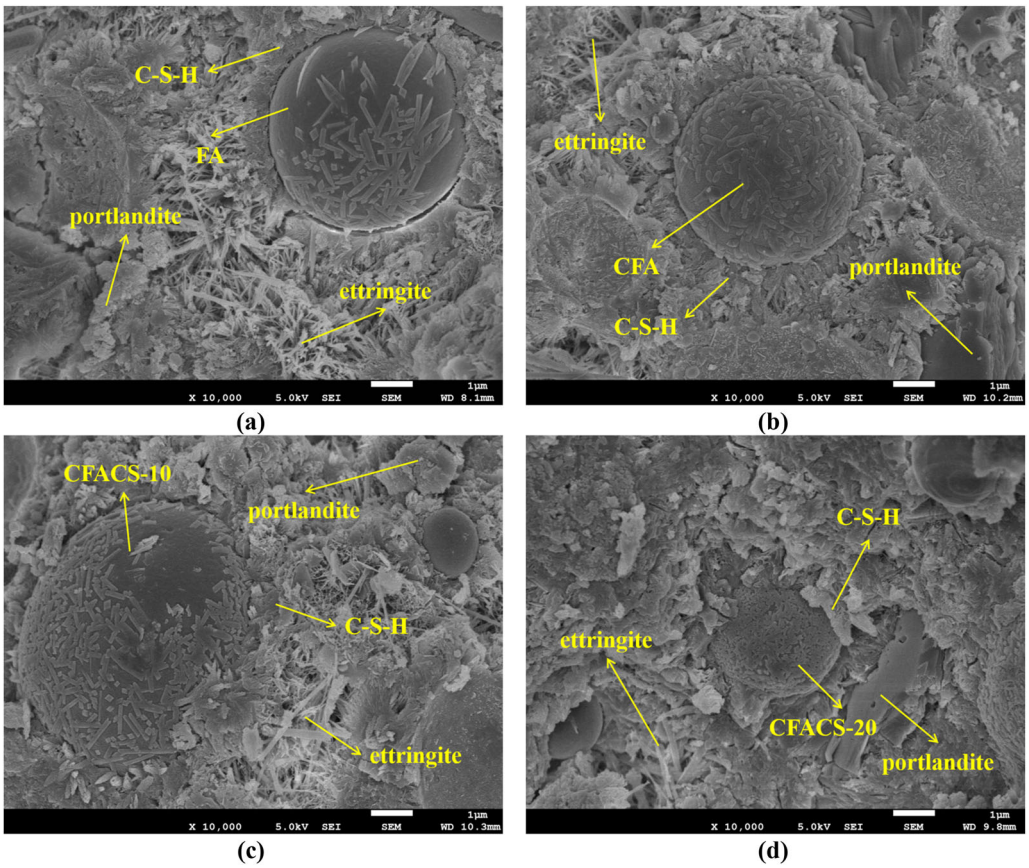

Figure 17. SEM images of cement pastes after 28 days of hydration: (a) OPC/FA; (b) OPC/CFA; (c) OPC/CFACS-10 and (d) OPC/CFACS-20.

aqueous approach. Morphology, particle size distribution, and chemical composition of the carbonated FAs were characterized and its performance as SCMs was investigated. The following conclusions can be drawn.

- A synergistic effect of FA coupled with CS for mineralization exists. This leads to a significant improvement on CO_2 uptake compared with the carbonation of CS and FA individually.
- The mineralization product mainly consists of calcite. Calcium carbonate particles with cubic shape nucleate on the FA surfaces and cluster further with the mineralization. This leads to the increased SSA.
- When used as SCMs, the carbonation treatment does not significantly increase the water requirement of FA but does effectively mitigate the set retardation in OPC/FA blends. The addition of CS for the carbonation treatment increases the 3 d and 28 d SAIs by 37.2% and 24.3%, respectively.
- The mineralized calcium carbonate alters the early hydration kinetics of binders from both physical and chemical mechanism. Evidence from the XRD, TGA, and SEM observations confirms that the dosage of mineralized calcium carbonate governs the ettringite preservation, carboaluminate formation and increase in hydration degree of cement clinker phases.

Using synergy carbonation treatment of FA and CS under normal temperatures and pressures to produce SCMs for high volume replacement of OPC can be a sustainable and economical solution for reducing the carbon footprint of the cement industry. This reduction results both from the mineralization process and the reduced cement clinker required for concrete production. Nevertheless, further research on the influence of carbonated FA on the durability and volume stability of blended cement is required for the popularization of the synergy carbonation technique.

Disclosure statement

No potential conflict of interest was reported by the author(s).

Funding

This work was supported by the Key Basic Research Project of China (No. 2022YFC3005604), 111 Project (No. B21012), National Natural Science Foundation of China (No. 52378250), Taishan Scholars Foundation of Shandong Province (No. tsqn201909032), Natural Science Foundation of Shandong Province (No. ZR2024ME113).

ORCID

Zhi Ge http://orcid.org/0000-0001-5719-5791

References

[1] Andrew RM. Global CO_2 emissions from cement production. Earth System Science Data. 2018;10(1):195–217. doi: 10.5194/essd-10-195-2018.

[2] Cao Y, Wang Y, Zhang Z, et al. Turning sandstone clay into supplementary cementitious material: activation and pozzolanic reactivity evaluation. Compos Part B Eng. 2021;223:109137. doi: 10.1016/j.compositesb.2021.109137.

[3] Izumi Y, Iizuka A, Ho H-J. Calculation of greenhouse gas emissions for a carbon recycling system using mineral carbon capture and utilization technology in the cement industry. J Clean Prod. 2021;312:127618. doi: 10.1016/j.jclepro.2021.127618.

[4] Abdulkareem OA, Ramli M, Matthews JC. Production of geopolymer mortar system containing high calcium biomass wood ash as a partial substitution to fly ash: an early age evaluation. Compos Part B Eng. 2019;174:106941. doi: 10.1016/j.compositesb.2019.106941.

[5] Monteiro PJ, Miller SA, Horvath A. Towards sustainable concrete. Nat Mater. 2017;16:698–699.

[6] Thomas BS, Yang J, Mo KH, et al. Biomass ashes from agricultural wastes as supplementary cementitious materials or aggregate replacement in cement/geopolymer concrete: a comprehensive review. J Build Eng. 2021;40:102332. doi: 10.1016/j.jobe.2021.102332.

[7] Amran M, Makul N, Fediuk R, et al. Global carbon recoverability experiences from the cement industry. Case Stud Constr Mater. 2022;17:e01439. doi: 10.1016/j.cscm.2022.e01439.

[8] Yin T, Yin S, Srivastava A, et al. Regenerable solvents mediate accelerated low temperature CO_2 capture and carbon mineralization of ash and nano-scale calcium carbonate formation. Resour Conserv Recycl. 2022;180:106209. doi: 10.1016/j.resconrec.2022.106209.

[9] Neves Junior A, Ferreira SR, Toledo Filho RD, et al. Effect of early age curing carbonation on the mechanical properties and durability of high initial strength Portland cement and lime–pozzolan composites reinforced with long sisal fibres. Compos Part B Eng. 2019;163:351–362. doi: 10.1016/j.compositesb.2018.11.006.

[10] Wang X-Y. Embodied CO_2-based optimal design of concrete with fly ash considering stress and carbonation. J Sustain Cem Based Mater. 2023;12(1):71–82. doi: 10.1080/21650373.2021.2015006.

[11] Pandey VC. Chapter 10 – an appraisal on phytomanagement of fly ash with economic returns. Phytomanagement of Fly Ash. 2020;10:289–321. doi:10.1016/B978-0-12-818544-5.00010-9.

[12] Moradian M, Hu Q, Aboustait M, et al. Direct in-situ observation of early age void evolution in sustainable cement paste containing fly ash or limestone. Compos Part B Eng. 2019;175:107099. doi: 10.1016/j.compositesb.2019.107099.

[13] Van den Heede P, De Belie N. Environmental impact and life cycle assessment (LCA) of traditional and 'green' concretes: literature review and theoretical calculations. Cem Concr Compos. 2012;34(4):431–442. doi: 10.1016/j.cemconcomp.2012.01.004.

[14] De Weerdt K, Haha MB, Le Saout G, et al. Hydration mechanisms of ternary Portland cements containing limestone powder and fly ash. Cem Concr Res. 2011;41(3):279–291. doi: 10.1016/j.cemconres.2010.11.014.

[15] Hemalatha T, Ramaswamy A. A review on fly ash characteristics – towards promoting high volume utilization in developing sustainable concrete. J Clean Prod. 2017;147:546–559. doi: 10.1016/j.jclepro.2017.01.114.

[16] Zou F, Hu C, Wang F, et al. Enhancement of early-age strength of the high content fly ash blended cement paste by sodium sulfate and C–S–H seeds towards a greener binder. J Clean Prod. 2020;244:118566. doi: 10.1016/j.jclepro.2019.118566.

[17] De Weerdt K, Kjellsen KO, Sellevold E, et al. Synergy between fly ash and limestone powder in ternary cements. Cem Concr Compos. 2011;33(1):30–38. doi: 10.1016/j.cemconcomp.2010.09.006.

[18] Bentz DP, Sato T, de la Varga I, et al. Fine limestone additions to regulate setting in high volume fly ash mixtures. Cem Concr Compos. 2012;34(1):11–17. doi: 10.1016/j.cemconcomp.2011.09.004.

[19] Thongsanitgarn P, Wongkeo W, Chaipanich A, et al. Heat of hydration of Portland high-calcium fly ash cement incorporating limestone powder: effect of limestone particle size. Constr Build Mater. 2014;66:410–417. doi: 10.1016/j.conbuildmat.2014.05.060.

[20] Sato T, Diallo F. Seeding effect of nano-$CaCO_3$ on the hydration of tricalcium silicate. Transp Res Rec. 2010;2141(1):61–67. doi: 10.3141/2141-11.

[21] Kawashima S, Hou P, Corr DJ, et al. Modification of cement-based materials with nanoparticles. Cem Concr Compos. 2013;36:8–15. doi: 10.1016/j.cemconcomp.2012.06.012.

[22] Shaikh FUA, Supit SWM. Mechanical and durability properties of high volume fly ash (HVFA) concrete containing calcium carbonate ($CaCO_3$) nanoparticles. Constr Build Mater. 2014;70:309–321. doi: 10.1016/j.conbuildmat.2014.07.099.

[23] Meng T, Yu Y, Wang Z. Effect of nano-$CaCO_3$ slurry on the mechanical properties and micro-structure of concrete with and without fly ash. Compos Part B Eng. 2017;117:124–129. doi: 10.1016/j.compositesb.2017.02.030.

[24] Liu W, Teng L, Rohani S, et al. CO_2 mineral carbonation using industrial solid wastes: a review of recent developments. Chem Eng J. 2021;416:129093. doi: 10.1016/j.cej.2021.129093.

[25] Monkman S, Kenward PA, Dipple G, et al. Activation of cement hydration with carbon dioxide. J Sustain Cem Based Mater. 2018;7(3):160–181. doi: 10.1080/21650373.2018.1443854.

[26] Palmqvist NGM, Nedelec J-M, Seisenbaeva GA, et al. Controlling nucleation and growth of nano-$CaCO_3$ via CO_2 sequestration by a calcium alkoxide solution to produce nanocomposites for drug delivery applications. Acta Biomater. 2017;57:426–434. doi: 10.1016/j.actbio.2017.05.006.

[27] Kitamura M. Crystallization and transformation mechanism of calcium carbonate polymorphs and the effect of magnesium ion. J Colloid Interface Sci. 2001;236(2):318–327. doi: 10.1006/jcis.2000.7398.

[28] Wang Y, Liu J, Hu X, et al. Utilization of accelerated carbonation to enhance the application of steel slag: a review. J Sustain Cem Based Mater. 2023;12(4):471–486. doi: 10.1080/21650373.2022.2154287.

[29] Pan S-Y, Chen Y-H, Fan L-S, et al. CO_2 mineralization and utilization by alkaline solid wastes for potential carbon reduction. Nat Sustain. 2020;3(5):399–405. doi: 10.1038/s41893-020-0486-9.

[30] Cetin B, Aydilek AH, Guney Y. Stabilization of recycled base materials with high carbon fly ash. Resour Conserv Recycl. 2010;54(11):878–892. doi: 10.1016/j.resconrec.2010.01.007.

[31] Wang Z, Xu S, Zheng S, et al. Accelerated carbonation and stabilization of BOF slag: data fitting relationship between particle size and CO_2 sequestration. J Sustain

Cem Based Mater. 2024;13(5):726–737. doi: 10.1080/21650373.2023.2301665.
[32] Hosseini Asl SM, Javadian H, Khavarpour M, et al. Porous adsorbents derived from coal fly ash as cost-effective and environmentally-friendly sources of aluminosilicate for sequestration of aqueous and gaseous pollutants: a review. J Clean Prod. 2019;208:1131–1147. doi: 10.1016/j.jclepro.2018.10.186.
[33] Siriruang C, Toochinda P, Julnipitawong P, et al. CO_2 capture using fly ash from coal fired power plant and applications of CO_2-captured fly ash as a mineral admixture for concrete. J Environ Manage. 2016;170:70–78. doi: 10.1016/j.jenvman.2016.01.010.
[34] Chen T, Bai M, Gao X. Carbonation curing of cement mortars incorporating carbonated fly ash for performance improvement and CO_2 sequestration. J CO2 Util. 2021;51:101633. doi: 10.1016/j.jcou.2021.101633.
[35] Li L, Wu M. An overview of utilizing CO_2 for accelerated carbonation treatment in the concrete industry. J CO2 Util. 2022;60:102000. doi: 10.1016/j.jcou.2022.102000.
[36] Ukwattage NL, Ranjith PG, Yellishetty M, et al. A laboratory-scale study of the aqueous mineral carbonation of coal fly ash for CO_2 sequestration. J Clean Prod. 2015;103:665–674. doi: 10.1016/j.jclepro.2014.03.005.
[37] Ji L, Yu H, Zhang R, et al. Effects of fly ash properties on carbonation efficiency in CO_2 mineralisation. Fuel Process Technol. 2019;188:79–88. doi: 10.1016/j.fuproc.2019.01.015.
[38] Liu W, Su S, Xu K, et al. CO_2 sequestration by direct gas–solid carbonation of fly ash with steam addition. J Clean Prod. 2018;178:98–107. doi: 10.1016/j.jclepro.2017.12.281.
[39] Ukwattage NL, Ranjith PG, Wang SH. Investigation of the potential of coal combustion fly ash for mineral sequestration of CO_2 by accelerated carbonation. Energy. 2013;52:230–236. doi: 10.1016/j.energy.2012.12.048.
[40] Montes-Hernandez G, Pérez-López R, Renard F, et al. Mineral sequestration of CO_2 by aqueous carbonation of coal combustion fly-ash. J Hazard Mater. 2009;161(2–3):1347–1354. doi: 10.1016/j.jhazmat.2008.04.104.
[41] Back M, Kuehn M, Stanjek H, et al. Reactivity of alkaline lignite fly ashes towards CO_2 in water. Environ Sci Technol. 2008;42(12):4520–4526. doi: 10.1021/es702760v.
[42] Ji L, Yu H, Wang X, et al. CO_2 sequestration by direct mineralisation using fly ash from Chinese Shenfu coal. Fuel Process Technol. 2017;156:429–437. doi: 10.1016/j.fuproc.2016.10.004.
[43] Tamilselvi Dananjayan RR, Kandasamy P, Andimuthu R. Direct mineral carbonation of coal fly ash for CO_2 sequestration. J Clean Prod. 2016;112:4173–4182. doi: 10.1016/j.jclepro.2015.05.145.
[44] Ebrahimi A, Saffari M, Milani D, et al. Sustainable transformation of fly ash industrial waste into a construction cement blend via CO_2 carbonation. J Clean Prod. 2017;156:660–669. doi: 10.1016/j.jclepro.2017.04.037.
[45] Zhang H, Xu Y, Gan Y, et al. Combined experimental and numerical study of uniaxial compression failure of hardened cement paste at micrometre length scale. Cem Concr Res. 2019;126:105925. doi: 10.1016/j.cemconres.2019.105925.
[46] Ma Z, Liao H, Cheng F. Synergistic mechanisms of steelmaking slag coupled with carbide slag for CO_2 mineralization. Int J Greenhouse Gas Control. 2021;105:103229. doi: 10.1016/j.ijggc.2020.103229.
[47] Ji L, Yu H, Yu B, et al. Insights into carbonation kinetics of fly ash from Victorian lignite for CO_2 sequestration. Energy Fuels. 2018;32(4):4569–4578. doi: 10.1021/acs.energyfuels.7b03137.
[48] Shao X, Qin B, Shi Q, et al. The impacts of CO_2 mineralization reaction on the physicochemical characteristics of fly ash: a study under different reaction conditions of the water-to-solid ratio and the pressure of CO_2. Energy. 2024;287:129676. doi: 10.1016/j.energy.2023.129676.
[49] Jaschik J, Jaschik M, Warmuziński K. The utilisation of fly ash in CO_2 mineral carbonation. Chem Process Eng. 2016;37(1):29–39. doi: 10.1515/cpe-2016-0004.
[50] Wang D, Fang Y, Zhang Y, et al. Changes in mineral composition, growth of calcite crystal, and promotion of physico-chemical properties induced by carbonation of β-C2S. J CO2 Util. 2019;34:149–162. doi: 10.1016/j.jcou.2019.06.005.
[51] Ćwik A, Casanova I, Rausis K, et al. Utilization of high-calcium fly ashes through mineral carbonation: the cases for Greece, Poland and Spain. J CO2 Util. 2019;32:155–162. doi: 10.1016/j.jcou.2019.03.020.
[52] Song X, Weng C, Cao Y, et al. Facile synthesis of pure vaterite using steamed ammonia liquid waste and ammonium carbonate without additives via simple mechanical mixing. Powder Technol. 2021;386:361–371. doi: 10.1016/j.powtec.2021.03.047.
[53] Poon CS, Shen P, Jiang Y, et al. Total recycling of concrete waste using accelerated carbonation: a review. Cem Concr Res. 2023;173:107284. doi: 10.1016/j.cemconres.2023.107284.
[54] Zhang Y, Yu L, Cui K, et al. Carbon capture and storage technology by steel-making slags: recent progress and future challenges. Chem Eng J. 2023;455:140552. doi: 10.1016/j.cej.2022.140552.
[55] Gomari KE, Gomari SR, Hughes D, et al. Exploring the potential of steel slag waste for carbon sequestration through mineral carbonation: a comparative study of blast-furnace slag and ladle slag. J Environ Manage. 2024;351:119835. doi: 10.1016/j.jenvman.2023.119835.
[56] Li Y, Eyley S, Thielemans W, et al. Valorization of deep soil mixing residue in cement-based materials. Resour Conserv Recycl. 2022;187:106597. doi: 10.1016/j.resconrec.2022.106597.
[57] Moorehead DR. Cementation by the carbonation of hydrated lime. Cem Concr Res. 1986;16(5):700–708. doi: 10.1016/0008-8846(86)90044-X.
[58] Karim M, Zain M, Jamil M, et al. Strength development of mortar and concrete containing fly ash: a review. Int J Phys Sci. 2011;6(17):4137–4153.
[59] Gardner LJ, Bernal SA, Walling SA, et al. Characterisation of magnesium potassium phosphate cements blended with fly ash and ground granulated blast furnace slag. Cem Concr Res. 2015;74:78–87. doi: 10.1016/j.cemconres.2015.01.015.
[60] Sato T, Beaudoin JJ. Effect of nano-$CaCO_3$ on hydration of cement containing supplementary cementitious materials. Adv Cem Res. 2011;23(1):33–43. doi: 10.1680/adcr.9.00016.
[61] Ramachandran VS. Influence of CaCO3 on hydration and microstructural characteristic of tricalcium silicate. I1 Cemento. 1986;3:129–152.
[62] Jansen D, Goetz-Neunhoeffer F, Lothenbach B, et al. The early hydration of ordinary Portland cement (OPC): an approach comparing measured heat flow with calculated heat flow from QXRD. Cem Concr Res. 2012;42(1):134–138. doi: 10.1016/j.cemconres.2011.09.001.
[63] Makar JM, Chan GW, Esseghaier KY. A peak in the hydration reaction at the end of the cement induction

period. J Mater Sci. 2007;42(4):1388–1392. doi: 10.1007/s10853-006-1427-3.
[64] Berodier E, Scrivener K. Understanding the filler effect on the nucleation and growth of C–S–H. J Am Ceram Soc. 2014;37(12):64–73.
[65] Avet F, Li X, Scrivener K. Determination of the amount of reacted metakaolin in calcined clay blends. Cem Concr Res. 2018;106:40–48. doi: 10.1016/j.cemconres.2018.01.009.
[66] Matschei T, Lothenbach B, Glasser FP. The AFm phase in Portland cement. Cem Concr Res. 2007;37(2):118–130. doi: 10.1016/j.cemconres.2006.10.010.
[67] Thongsanitgarn P, Wongkeo W, Chaipanich A. Hydration and compressive strength of blended cement containing fly ash and limestone as cement replacement. J Mater Civ Eng. 2014;26(12):04014088. doi: 10.1061/(ASCE)MT.1943-5533.0001002.
[68] Zajac M, Rossberg A, Le Saout G, et al. Influence of limestone and anhydrite on the hydration of Portland cements. Cem Concr Compos. 2014;46:99–108. doi: 10.1016/j.cemconcomp.2013.11.007.
[69] Matschei T, Lothenbach B, Glasser PF. The role of calcium carbonate in cement hydration. Cem Concr Res. 2007;37(4):551–558. doi: 10.1016/j.cemconres.2006.10.013.
[70] Lothenbach B, Saout GL, Gallucci E, et al. Influence of limestone on the hydration of Portland cements. Cem Concr Res. 2008;38(6):339–356.
[71] Li Y, Mi T, Liu W, et al. Chemical and mineralogical characteristics of carbonated and uncarbonated cement pastes subjected to high temperatures. Compos Part B Eng. 2021;216:108861. doi: 10.1016/j.compositesb.2021.108861.
[72] Scrivener K, Snellings R, Lothenbach B. A practical guide to microstructural analysis of cementitious materials. Boca Raton (FL): CRC Press; 2016.
[73] Shah V, Scrivener K, Bhattacharjee B, et al. Changes in microstructure characteristics of cement paste on carbonation. Cem Concr Res. 2018;109:184–197. doi: 10.1016/j.cemconres.2018.04.016.
[74] Dhandapani Y, Santhanam M, Kaladharan G, et al. Towards ternary binders involving limestone additions—a review. Cem Concr Res. 2021;143:106396. doi: 10.1016/j.cemconres.2021.106396.
[75] Herath C, Gunasekara C, Law DW, et al. Performance of high volume fly ash concrete incorporating additives: a systematic literature review. Constr Build Mater. 2020;258:120606. doi: 10.1016/j.conbuildmat.2020.120606.
[76] Medjigbodo G, Rozière E, Charrier K, et al. Hydration, shrinkage, and durability of ternary binders containing Portland cement, limestone filler and metakaolin. Constr Build Mater. 2018;183:114–126. doi: 10.1016/j.conbuildmat.2018.06.138.
[77] Georget F, Lothenbach B, Wilson W, et al. Stability of hemicarbonate under cement paste-like conditions. Cem Concr Res. 2022;153:106692. doi: 10.1016/j.cemconres.2021.106692.
[78] Zhao X-G, Wu S, Wang L, et al. Analysis of Pore Structure of Rice Husk Ash Concrete Under Freeze-Thaw Cycling. Integrated Ferroelectrics. 2024;240(3):599–612. doi: 10.1080/10584587.2024.2324686.
[79] Moghaddam F, Sirivivatnanon V, Vessalas K. The effect of fly ash fineness on heat of hydration, microstructure, flow and compressive strength of blended cement pastes. Case Stud Constr Mater. 2019;10:e00218. doi: 10.1016/j.cscm.2019.e00218.
[80] Lothenbach B, Matschei T, Schner GRM, et al. Thermodynamic modelling of the effect of temperature on the hydration and porosity of Portland cement. Cem Concr Res. 2008;38(1):1–18. ? doi: 10.1016/j.cemconres.2007.08.017.
[81] Yang H, Che Y, Leng F. High volume fly ash mortar containing nano-calcium carbonate as a sustainable cementitious material: microstructure and strength development. Sci Rep. 2018;8(1):16439. doi: 10.1038/s41598-018-34851-4.
[82] L'Hôpital E, Lothenbach B, Kulik DA, et al. Influence of calcium to silica ratio on aluminium uptake in calcium silicate hydrate. Cem Concr Res. 2016;85:111–121. doi: 10.1016/j.cemconres.2016.01.014.